PROCEEDINGS OF SCIENCE

Scattering Observables from Few-Body Densities and Application in Light Nuclei

Alexander Long* **and Harald W. Grießhammer**

Institute for Nuclear Studies, Department of Physics,
The George Washington University

E-mail: alexlong@gwu.edu, hgrie@gwu.edu

The dynamics of scattering on light nuclei is well understood, but its calculation is numerically difficult using standard methods. Fortunately, using recent developments, the relevant quantities can be factored into a product of the n-body transition density amplitude (TDA) and the interaction kernel of a chosen probe. These TDAs depend only on the target, and not the probe; they are calculated once and stored. The kernels depend on only the probe and not the target, they can be reused for different targets. The calculation of the transition densities becomes numerically difficult for $n \geq 4$, but we discuss a solution through use of a renormalization group transformation. This technique allows for extending the TDA method to ^{6}Li. We present preliminary results for Compton scattering on ^{6}Li and compare with available data. We also discuss extension to pion-photoproduction and other reactions.

The 11th International Workshop on Chiral Dynamics (CD2024)
26-30 August 2024
Ruhr University Bochum, Germany

*Speaker

 ISSN 1824-8039 . Published by SISSA Medialab.

This is a comment, (for Dr.Griesshammer's use) a^2 *This is a question (for Alex's use)*

1. Introduction

Effective field theories (EFTs) in nuclear physics provide a framework for making precise predictions by employing only those degrees of freedom that are most pertinent to the physical system under consideration, rather than relying on the complete set of intrinsic degrees of freedom present in the underlying theory (typically quarks and gluons). In this work, we utilize chiral effective field theory which adopts hadrons as its fundamental degrees of freedom. The present study is concerned with the scattering of probes off light nuclei. To this end, the transition density approximation (TDA) method was developed by Grießhammer *et al.* and de Vries *et al.* [1, 17]. The TDA formalism describes the interaction of a probe with an A-body target. Consequently, the probe may interact with up to A nucleons. The n nucleons with which the probe interacts are designated as *active*, whereas the remaining $A - n$ nucleons are referred to as *spectators*. The mathematical treatment of these two components is entirely distinct: the active n nucleons contribute to the n-body kernel, while the spectator nucleons contribute to n-body the TDA.

The n-body kernel characterizes the interaction in reduced case in which the probe interacts exclusively with the n-body system. For example, the one-body kernel in Compton scattering encompasses the same contributions as those arising in Compton scattering off a single nucleon. This complete separation of the contributions implies that if one has access to a distinct kernels and b distinct TDAs, then a total of ab different outcomes may be generated. Figure 1 provides an illustrative example for the case $A = 3$.

For scattering off an A-body nucleus, the total scattering amplitude is given by *you want a citation here but I think I am the first person to actually write this down. I can cite the* ^{3}He *paper if you want.*

$$A_M^{M'}(\vec{k},\vec{q}) = \binom{A}{1}\langle M'|\,\hat{O}_1(\vec{k},\vec{q})\,|M\rangle + \binom{A}{2}\langle M'|\,\hat{O}_2(\vec{k},\vec{q})\,|M\rangle \quad +\ldots+ \binom{A}{A}\langle M'|\,\hat{O}_A(\vec{k},\vec{q})\,|M\rangle \tag{1}$$

$$A_M^{M'}(\vec{k},\vec{q}) = \left\langle M'\left|\binom{A}{1}\hat{O}_1(\vec{k},\vec{q}) + \binom{A}{2}\hat{O}_2(\vec{k},\vec{q}) + \ldots + \binom{A}{A}\hat{O}_A(\vec{k},\vec{q})\right|M\right\rangle \tag{2}$$

where $\hat{O}_i$ is the i-body kernel, M, M' is the spin projection of the target nucleus, and there are $\binom{A}{i}$ ways for a probe to hit i nucleons. Fortunately, χEFT provides a hierarchy of scales which predicts decreasing contributions for higher order terms for probe energies greater than $\sim$ 40MeV. Therefore, the 3-body contribution and higher is negligible at this order, and we simply use

$$A_M^{M'}(\vec{k},\vec{q}) = \binom{A}{1}\langle M'|\,\hat{O}_3(\vec{k},\vec{q})\,|M\rangle + \binom{A}{2}\langle M'|\,\hat{O}_2(\vec{k},\vec{q})\,|M\rangle$$

In practice this is enough for accuracy on roughly the 5% level.

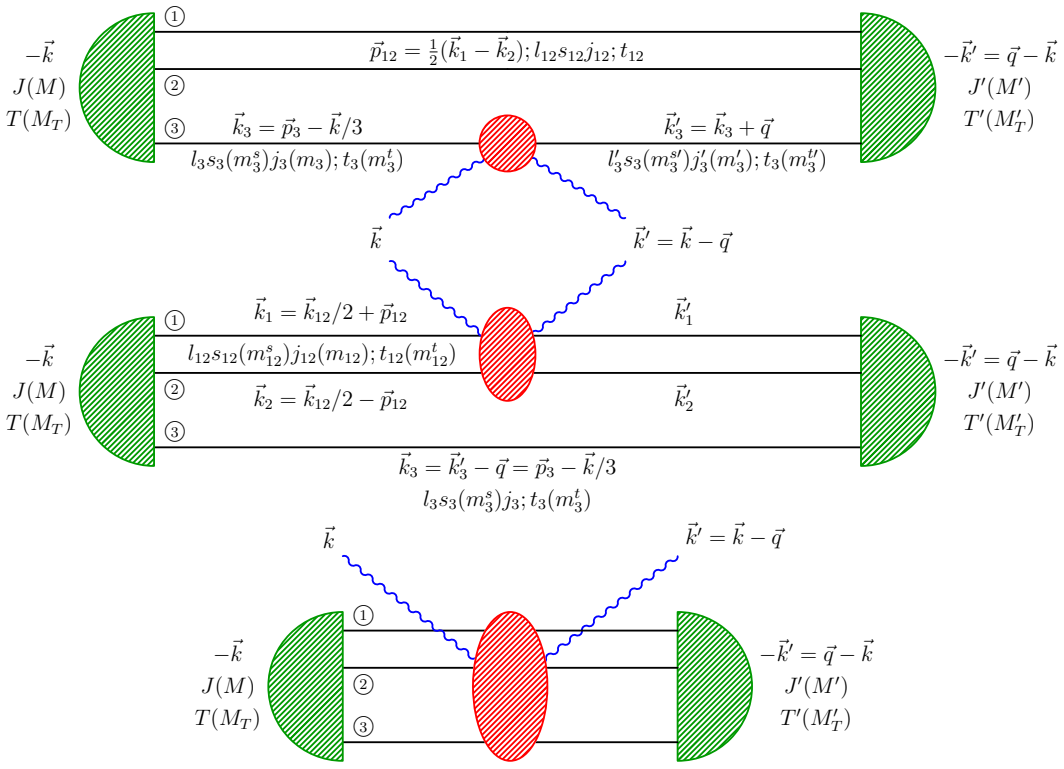

Figure 1: Kinematics in the center of mass frame and quantum numbers for an $A = 3$ system in the case of Compton scattering. Generalization to other reactions only changes the kind of ingoing/outgoing probe. Generalization to $A > 3$ would result in more internal lines representing the nucleons. Top: one-body processes $\hat{O}_1$, center: two-body processes $\hat{O}_2$, bottom: three-body processes $\hat{O}_3$. Red represents the kernels; everything else is represented by the densities. Green represents the wavefunction of the nucleons. From Grießhammer *et al.*[1]

2. Kernels and Densities

The one-body and two-body kernel must be considered separately. Their form is different, and they require a one- and two-body density respectively. Symbolically, the matrix element $\hat{O}_3$ is:

$$\begin{aligned}\left\langle M' \left| \hat{O}_1(\vec{k},\vec{q}) \right| M \right\rangle = \sum_{\alpha\alpha'} \int \mathrm{d}p_{12} p_{12}^2 \, \mathrm{d}p_3 p_3^2 \, \mathrm{d}p'_{12} p'^2_{12} \, \mathrm{d}p'_3 p'^2_3 \psi^\dagger_{\alpha'} \left(p'_{12} p'_3\right) \psi_\alpha \left(p_{12} p_3\right) \\ \times \left\langle p'_{12} p'_3 \left[\left(l'_{12} s'_{12}\right) j'_{12} \left(l'_3 s_3\right) j'_3 \right] J'M' \left(t'_{12} t_3\right) T'M_T \right| \hat{O}_1(\vec{k},\vec{q}) \\ \left| p_{12} p_3 \left[\left(l_{12} s_{12}\right) j_{12} \left(l_3 s_3\right) j_3 \right] JM \left(t_{12} t_3\right) TM_T \right\rangle .\end{aligned} \tag{3}$$

The central result is that up to relativistic corrections, this can be written as:

$$\left\langle M' \left| \hat{O}_1(\vec{k},\vec{q}) \right| M \right\rangle = \sum_{\substack{m_3^{s\prime} m_3^s \\ m_3^t}} \hat{O}_1 \left(m_3^{s\prime} m_3^s, m_3^t; \vec{k}, \vec{q} \right) \rho^{m_3^t M_T, M'M}_{m_3^{s\prime} m_3^s} (\vec{k},\vec{q}) \, . \tag{4}$$

For full details see Greißhammer *et al.*[1]. Here ρ, is the *one-body transition density amplitude* (TDA) for the nucleus which was discussed previously and can truly be interpreted as the probability

amplitude that nucleon m_3^t absorbs momentum $\vec{q}$, changes its spin projection from m_s^3 to $m_s^{3'}$ and changes the spin-projection of the nucleus from M to M'. Its operator form is

$$\rho^{m_3^t M_T, M'M}_{m_3' m_3^s}(\vec{k}, \vec{q}) = \langle M' \left| s_3 m_3^{s\prime}, t_3 m_3^t \right\rangle \mathrm{e}^{\mathrm{i}\frac{2}{3}\vec{q}\cdot\vec{r}_3} \left\langle s_3 m_3^s, t_3 m_3^t \right| M \rangle \,. \tag{5}$$

The two body case works similarly, and results in

$$\left\langle M' \left| \hat{O}_2 \right| M \right\rangle = \sum_{\alpha_{11}', \alpha_{12}} \int \mathrm{d}p_{12}\, p_{12}^2\, \mathrm{d}p_{12}'\, p_{12}'^2\, O_2^{\alpha_{12}'\alpha_{12}}\left(p_{12}', p_{12}\right) \rho^{M_T, M'M}_{\alpha_{12}'\alpha_{12}}\left(p_{12}', p_{12}; \vec{q}\right) \,. \tag{6}$$

This is the two-body equivalent to (4). There is an expression analogous to (3) but it is non-trivial and for our purposes non-enlightening. This two-body density $\rho^{M_T, M'M}_{\alpha_{12}'\alpha_{12}}$ is of course distinct from the one-body density. Moreover, just like the one-body case, it can also be interpreted as a probability density. It depends on the incoming and outgoing quantum numbers α_{12} and α_{12}' of the 1-2 system, and also on the initial and final relative momenta $p_{12} and p_{12}'$ of the two nucleons which are integrated over. As a result, the file size for the two nucleon densities is approximately 20 MiB per energy and angle, whereas those of the one nucleon densities are on the order of a few KB. Importantly, ρ can be computed directly from a nuclear potential, such as the chiral SMS potential [2] without reference to the kernel $\hat{O}_1$ or $\hat{O}_2$.

3. SRG Transformation

Previous work using the TDA formalism has analyzed ^{3}He and ^{4}He [1, 3] , but to extend this to ^{6}Li involves many-body interactions which are much more complicated and computationally expensive. To make the calculation of a TDA feasible for $A = 6$, a *similarity renormalization group* (SRG) transformation is employed [4, 15]. This is of much experimental interest since ^{6}Li is a stable solid at room temperature and is therefore relatively simple to conduct an experiment on, even to high precision due to its relatively large cross section and count rate. There have been many experiments on ^{6}Li [10, 11], yet to date there is no theory prediction, we seek to fill in this gap. When using nuclear potentials, we approximate the nucleon-nucleon potential to be zero beyond a certain cutoff Λ_{NN}, and consequently neglect contributions above this cutoff in our calculations. In general, a nuclear potential, such as the chiral SMS potential does not fall off rapidly at high momenta [2]. As a result we would have to extend the cutoff Λ_{NN} much further than is desirable, which in turn increases computational cost. The SRG transformation is a unitary transformation that shifts the relevant physics into the low-momentum region, thereby lowering minimum effective Λ_{NN} in the SRG evolved space. This, in turn, significantly improves the convergence rate of calculations for $A = 6$. The SRG transformation can be thought of as a local averaging or smoothing of the potential, resulting in decreased resolution has the SRG is applied.

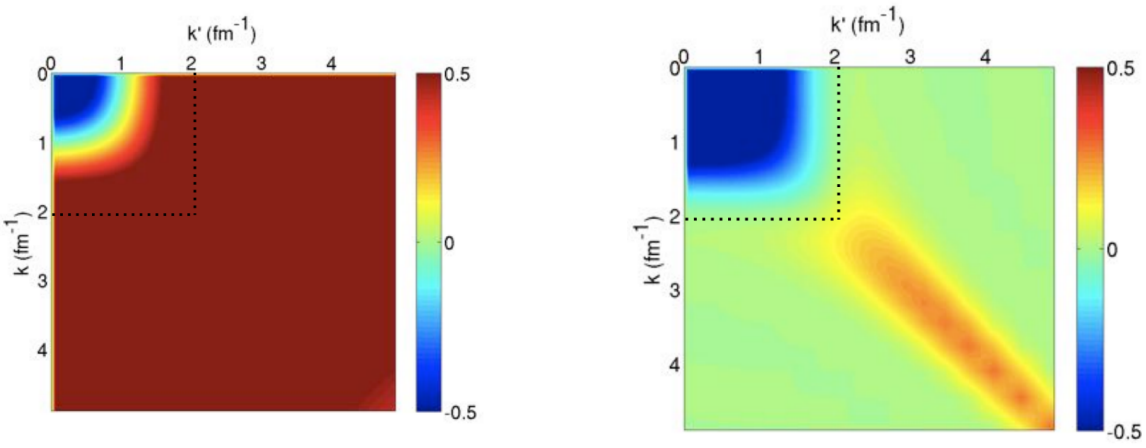

(a) High Resolution (before much SRG is applied)

(b) Low Resolution (evolved)

Figure 2: Nuclear potentials $V(k, k')$. Figures from Kai Hebeler: "Chiral Effective Field Theory and Nuclear Forces: overview and applications" presentation at TALENT school at MITP 2022, and modified with permission from Furnstahl *et al.*[15].

In the under-evolved, high resolution figure 2a the potential does not go to zero rapidly, whereas it does once the transformation is applied in figure 2b. As a result a cutoff can be made at $\Lambda_{\text{NN}} = 2\text{fm}^{-1}$ without losing much accuracy whereas the under-evolved potential required at least $\Lambda_{\text{NN}} = 5\text{fm}^{-1}$. The time complexity is at minimum proportional to the number of array elements present, therefore we gain a factor of $(5/2)^2 = 6.25$ in efficiency; in practice the gains are even higher.

The SRG transformation is essential, but it also creates a change in the physical meaning of the free variables. In fact, any unitary transformation ($U^\dagger U = \mathbb{1}$) also transforms the coordinates.

$$\langle p' | V | p \rangle = \langle p' | U^\dagger U V U^\dagger U | p \rangle = \langle p' | U^\dagger \left(U V U^\dagger \right) U | p \rangle = \langle \widetilde{p}' | V_{eff} | \widetilde{p} \rangle = V_{eff}(\widetilde{p}, \widetilde{p}') \quad (7)$$

So referring to the free variables in an SRG-transformed potential as "momenta" is, to some extent, incorrect. They do not represent physical states in the sense that they are not eigenstates to physical momenta. The Lagrangeans that generate the Feynman diagrams in the kernel, however, depend on physical momenta, and therefore we cannot directly use an SRG evolved potential in the non-SRG evolved kernel. To solve this, previous work with SRG transformations has transformed the Lagrangeans - and therefore the kernels - into the SRG evolved space as well *get citation* . However, in the context of the density formalism this would mean adding SRG dependence into the kernel, thereby breaking kernel-density independence. Additionally, the SRG transformation can take many different forms [4, 15]; we wish to allow for these developments without having to re-write the kernel code. Therefore we have chosen to apply an inverse transformation to the densities [16].

The SRG evolution has parameters that must be fine-tuned, but this allows for uncertainty estimation. In particular, one must solve for the nucleus wavefunction; to this end an expansion in the harmonic oscillator basis is used. When expanded to infinite order, this basis forms a complete set, however, we truncate this expansion by including harmonic oscillator excitations up to N_{tot}. Additionally, the harmonic oscillator basis has a characteristic width, denoted by ω_H, and finally, the

parameter Λ_{SRG} represents the evolution of the potential, as seen in figure 2. $\Lambda_{\text{SRG}} = \infty$ corresponds to no evolution. All of these parameters affect the resulting cross-section. We note that uncertainty decreases monotonically with increasing N_{tot}, and at $N_{\text{tot}} = \infty$ the associated uncertainty goes to zero. Applying a stronger SRG evolution (lower Λ_{SRG}) to the potential results in larger induced many-body forces; however, we show in figure 3 the effect of this uncertainty is small. These induced forces exist because due to the cutoff Λ_{NN} the SRG transformation is only approximately unitary. Fortunately, when the TDA is calculated we also gain access to the binding energy of the simulated system. From this, we can estimate required values for ω_H and N_{tot} by comparing the experimental binding energy to computed binding energy. In order to gain confidence we first applied this methodology to ^{4}He, where we can compare SRG and non-SRG evolved results. With this completed we have now moved to ^{6}Li where we only have access to the SRG evolved form.

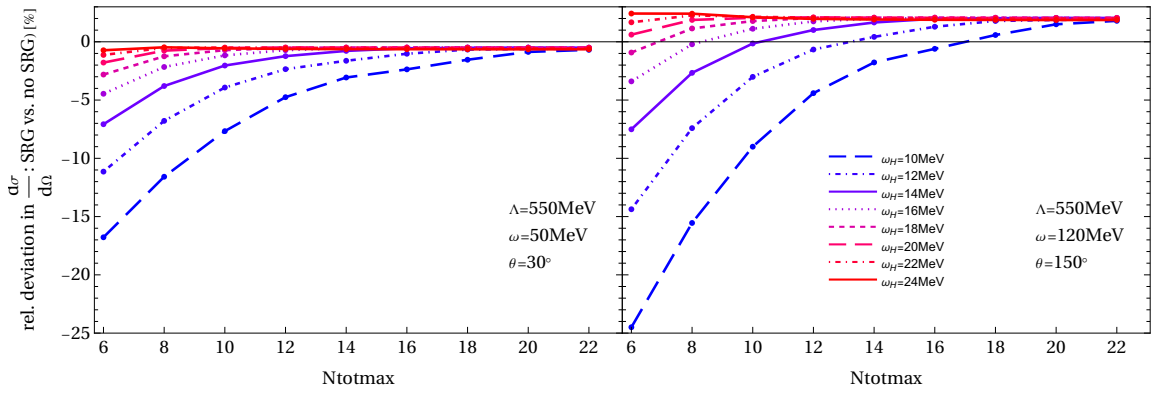

Figure 3: ^{4}He Compton scattering SRG convergence

$$\text{“Relative deviation, (Rel. deviation) of } A \text{ from } M\text{”} := \frac{A}{M} - 1 \tag{8}$$

In figure 3, we see the effectiveness of the results in the ^{4}He case. We expect the deviation to decrease as N increases, and importantly for our analysis, this shows what value of N is required. The small error present at high N_{tot} is present do to the induced many body forces.

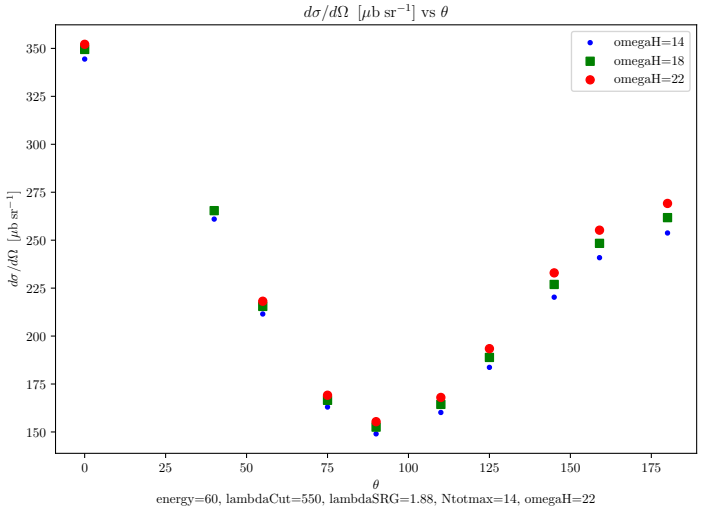

Figure 4: Caption

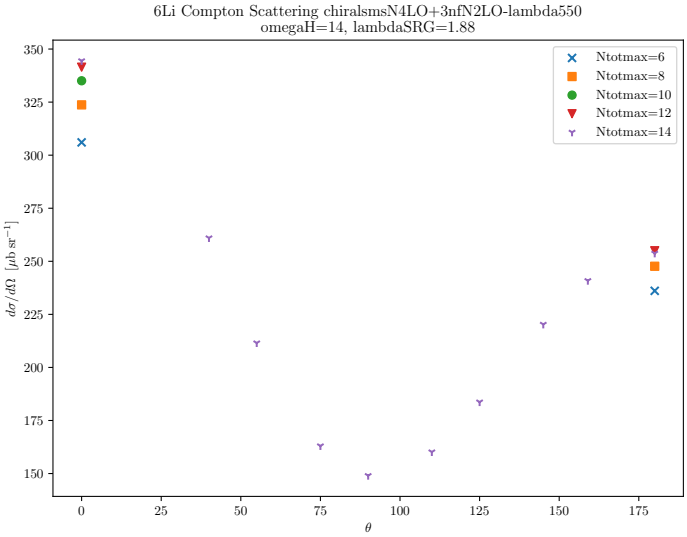

Figure 5: Caption

4. Using TDAs in different processes

With the TDAs calculated for Compton scattering, we now wish to recycle them for new processes. In particular pion-photoproduction, and pion scattering are of interest. Fortunately their kernels share remarkable similarity since if one ignores the type of incoming/outgoing particle the processes are topologically identical.

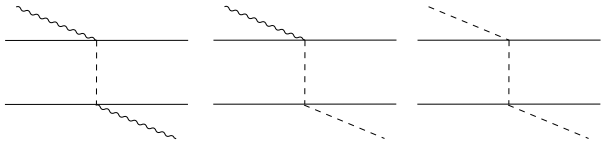

Figure 6: Topologically identical diagrams in Compton scattering, pion-photoproduction, and pion scattering

4.1 Pion-Photoproduction

For the pion-photoproduction one-body kernel, we use the results from a single nucleon scattering, $\gamma N \rightarrow \pi N$ which has been studied extensively [5, 7, 13, 14]. Its differential cross section can be decomposed into the electric and magnetic multipoles $E_{l\pm}, M_{l\pm}$ [5]. Over the years, many experimental results have measured these multipoles to high order and with good precision [6]. The resulting scattering matrices $\mathcal{M}$ are exactly what enters as $\hat{O}_1$ in equation (4). This approach solves a significant problem since the calculation of the one-body pion-photoproduction kernel to high accuracy directly from Feynman diagrams requires including many terms in the chiral expansion due to the proximity of the $\Delta(1232)$ resonance at $\sim$ 200MeV [7].

The two-body contributions do not easily decompose into multipoles , therefore we perform the calculation through expansions in the chiral Lagrangean through calculation of Feynman diagrams. It is likely this will lead to large uncertainties, as in the one-body case. At threshold energy, this reaction kernel has been analyzed by Lenkewitz *et al.*[8, 9]. We now have a numerically stable result for ^{3}He and seek to extend this approach to new targets. *Include some numbers, need to discuss with you uncertainty analysis.*

4.2 Pion scattering and other reactions

Beane *et al.*have developed the pion-pion kernel at threshold for both one-body and two-body interactions [12]. We may extend this analysis to finite energy. Once the pion-photoproduction and pion-pion scattering kernels have successfully been developed, we will be able to calculate all of these reactions on previously analyzed targets in the density formalism since we already have produced the TDAs required. In particular, we will calculate all of these reactions with the targets ^{3}H, ^{3}He, ^{4}He, and ^{6}Li.

5. Conclusion

We have developed and demonstrated a comprehensive framework for computing scattering observables in light nuclei by factorizing the full amplitude into target-dependent few-body transition density amplitudes (TDAs) and probe-dependent interaction kernels. This separation allows us to treat the nuclear structure and the reaction mechanism independently, thereby streamlining the calculation of observables. The central achievement of this work is the successful extension of the density formalism to heavier targets like ^{6}Li by incorporating a similarity renormalization group (SRG) transformation. The SRG not only accelerates the convergence of our calculations by lowering the effective momentum cutoff, but—when combined with an appropriate inverse

transformation of the densities—also preserves the kernel–density independence that is crucial for the versatility of our approach. Furthermore, we have presented the computation of Compton scattering on ^{6}Li which agrees well with data and we have outlined the extension of the formalism to other reactions, such as pion-photoproduction and pion-pion scattering. The ability to plug in different reaction kernels into the same TDA framework not only enhances the predictive power of our approach but also paves the way for a unified treatment of various scattering processes in few-body systems. Ultimately, this framework provides a promising route toward high-precision theoretical predictions, deepening our understanding of nuclear dynamics in light nuclei.

References

[1] H. W. Grießhammer, J. A. McGovern, A. Nogga, and D. R. Phillips, "Scattering Observables from One- and Two-body Densities: Formalism and Application to γ^3 Scattering," *Few-Body Systems*, vol. 61, no. 4, Nov. 2020. DOI: 10.1007/s00601-020-01578-w.

[2] P. Reinert, H. Krebs, and E. Epelbaum, "Semilocal momentum-space regularized chiral two-nucleon potentials up to fifth order," *The European Physical Journal A*, vol. 54, no. 5, May 2018. DOI: 10.1140/epja/i2018-12516-4.

[3] Grießhammer, H.W., Liao, J., McGovern, J.A. et al. Compton scattering on with nuclear one- and two-body densities. Eur. Phys. J. A 60, 132 (2024). https://doi.org/10.1140/epja/s10050-024-01339-x arXiv:2401.16995.

[4] S. Szpigel and R. J. Perry, "The Similarity Renormalization Group,", Quantum Field Theory: A Twentieth Century Profile, Sep. 2000. https://doi.org/10.48550/arXiv.hep-ph/0009071

[5] R. L. Walker, "Phenomenological Analysis of Single-Pion Photoproduction," *Phys. Rev.*, vol. 182, no. 5, pp. 1729–1748, Jun. 1969. DOI: 10.1103/PhysRev.182.1729.

[6] R. L. Workman, M. W. Paris, W. J. Briscoe, and I. I. Strakovsky, "Unified Chew-Mandelstam SAID analysis of pion photoproduction data," *Phys. Rev. C*, vol. 86, no. 1, p. 015202, Jul. 2012. DOI: 10.1103/PhysRevC.86.015202.

[7] N. Rijneveen, A. M. Gasparyan, H. Krebs, and E. Epelbaum, "Pion photoproduction in chiral perturbation theory with explicit treatment of the $\Delta(1232)$ resonance," *Phys. Rev. C*, vol. 106, no. 2, p. 025202, Aug. 2022. DOI: 10.1103/PhysRevC.106.025202.

[8] M. Lenkewitz, E. Epelbaum, H.-W. Hammer, and U.-G. Meißner, "Neutral pion photoproduction off ^{3}H and ^{3}He in chiral perturbation theory," *Physics Letters B*, vol. 700, no. 5, pp. 365–368, Jun. 2011. DOI: 10.1016/j.physletb.2011.05.036.

[9] M. Lenkewitz, E. Epelbaum, H.-W. Hammer, and U.-G. Meissner, "Threshold neutral pion photoproduction off the tri-nucleon to $O(q^4)$," *The European Physical Journal A*, vol. 49, no. 2, Feb. 2013. DOI: 10.1140/epja/i2013-13020-1.

[10] L. S. Myers, M. W. Ahmed, G. Feldman, A. Kafkarkou, D. P. Kendellen, I. Mazumdar, J. M. Mueller, M. H. Sikora, H. R. Weller, and W. R. Zimmerman, "Compton scattering from

^{6}Li at 86 MeV," *Phys. Rev. C*, vol. 90, no. 2, p. 027603, Aug. 2014. DOI: 10.1103/PhysRevC.90.027603.

[11] L. S. Myers, M. W. Ahmed, G. Feldman, S. S. Henshaw, M. A. Kovash, J. M. Mueller, and H. R. Weller, "Compton scattering from ^{6}Li at 60 MeV," *Phys. Rev. C*, vol. 86, no. 4, p. 044614, Oct. 2012. DOI: 10.1103/PhysRevC.86.044614.

[12] S. R. Beane, V. Bernard, E. Epelbaum, U.-G. Meißner, and D. R. Phillips, "The S-wave pion–nucleon scattering lengths from pionic atoms using effective field theory," *Nuclear Physics A*, vol. 720, no. 3–4, pp. 399–415, Jun. 2003. DOI: 10.1016/S0375-9474(03)01008-X.

[13] R. L. Workman, M. W. Paris, W. J. Briscoe, and I. I. Strakovsky, "Unified Chew-Mandelstam SAID analysis of pion photoproduction data," *Phys. Rev. C*, vol. 86, no. 1, p. 015202, Jul. 2012. DOI: 10.1103/PhysRevC.86.015202.

[14] W. J. Briscoe, A. Schmidt, I. Strakovsky, R. L. Workman, and A. Švarc, "Extended SAID partial-wave analysis of pion photoproduction," *Phys. Rev. C*, vol. 108, no. 6, p. 065205, Dec. 2023. DOI: 10.1103/PhysRevC.108.065205.

[15] R. J. Furnstahl and K. Hebeler, "New applications of renormalization group methods in nuclear physics," *Reports on Progress in Physics*, vol. 76, no. 12, p. 126301, Nov. 2013. DOI: 10.1088/0034-4885/76/12/126301.

[16] X.-X. Sun, H. Le, A. Nogga, and U.-G. Meißner, in preparation (2025).

[17] J. de Vries, C. Körber, A. Nogga, et al., "Dark matter scattering off He in chiral effective field theory," *Eur. Phys. J. C*, vol. 84, p. 1138, 2024. DOI: 10.1140/epjc/s10052-024-13477-z.